Structural connectivity mapping in human hippocampal-subfields using super-resolution hybrid diffusion imaging: a feasibility study

Nahla Elsaid, Pierrick Coupé, Andrew Saykin, Yu-Chien Wu

Structural Connectivity Mapping in Human Hippocampal-Subfields Using Super-Resolution Hybrid Diffusion Imaging: A Feasibility Study.

Abstract

Purpose The goal of the current study was to introduce a new methodology that holds a promise to be used in hippocampus-aging studies using sub-millimeter super-resolution hybrid diffusion imaging (HYDI) MRI.

Methods HYDI diffusion data were acquired in two groups of older and younger healthy participants recruited from the Indiana Alzheimer's Disease Research Center and community. These data were then transformed into super-resolution diffusion images before the hippocampal subfield analyses. We studied the correlation between the subjects' age and the structural connectivity involving the hippocampal subfields and the connectivity between the whole hippocampus and the cerebral cortex.

Results Structural integrity derived from the tractography streamlines between the hippocampal subfields was reduced in older than younger adults.

Conclusion The findings offered a new promising framework, and they opened avenues for future studies to explore the relationship between the structural connectivity in the hippocampal area and different types of dementia.

Keywords: normal aging, structural connectivity, diffusion imaging, hippocampal subfields, super-resolution

Introduction

The aging process is known to cause morphological and structural alterations in the human brain. Most of the previous studies that examined the effect of disease-free aging focused on measuring the correlation between brain volume and age. Some of these studies were cross-sectional volumetric studies examining the volumetric differences of a younger group versus an older group of healthy individuals [1,2]. Other aging studies were longitudinal, where the volumetric brain changes, covering the whole adult lifespan, were studied in a group of individuals who remained free of cognitive impairments longitudinally [3-6]. A few of these studies suggested that these volumetric changes are selective to some brain regions, e.g., the hippocampus, more than others [4,6].

As the hippocampus is one of the most vulnerable regions related to the aging process [7], several studies focused on the volumetric changes in the hippocampus as a whole entity [8]. Others showed regional variations in each of the hippocampal subfields [9]. The hippocampal subfields include the cornu-ammonis (CA1-4), the dentate gyrus (DG), and the subiculum (SUB). Other closely related structures adjacent to the hippocampus are not considered part of it. These include the entorhinal cortex (ERC), the parahippocampal cortex (PHC), the perirhinal cortex Brodmann areas 35 and 36 (BA35 and BA36). While being structurally and functionally distinct [10], due to their small sizes, the hippocampal subfields are difficult to image using conventional techniques.

The recent advancements in high-resolution anatomical magnetic resonance imaging (MRI) such as T1-weighted (T1W) or T2-weighted (T2W) imaging have enabled the feasibility of the submillimeter in-plane resolution of the hippocampus. These high resolution anatomical scans facilitate the manual/automatic segmentation of the hippocampal subfields [5,11-16]. On the

other hand, diffusion MRI could better delineate structural changes by revealing the structural connectivity between the hippocampal subfields. There are very few previous studies that investigated the use of high-resolution diffusion MRI without compromising the signal-to-noise ratio (SNR). One study resorted to higher in-plane resolution (0.664 mm) with a 3 mm slice thickness [15], and another study could reach 1.4 mm isotropic resolution [17]. Nevertheless, isotropic resolution of the DWIs is preferable and critical for accurately estimating the diffusion tractography streamlines [18,19].

One of the main challenges in previous studies of the hippocampal subfields is increasing the spatial resolution of diffusion MRI. Most of these studies focused on using diffusion tensor imaging (DTI) to study microstructural degradation due to aging. However, in normal DTI, partial volume effects (PVE) obstruct the correct estimation of FA in gray matter (only possible in white matter). However, through the super-resolution DWIs (which could mitigate the PVE), FA calculation within the gray matter can be more accurate. While DTI is a reliable diffusion reconstruction method, it cannot delineate the crossing pathways that might be present in the hippocampal structures. With the appropriate spatial resolution, diffusion MRI could provide microstructural measurements and associated tractography within the in-vivo human hippocampal subfields.

This study investigates the feasibility of a super-resolution pipeline that can highlight the aging differences in the hippocampus more than their average resolution counterparts. To achieve super-resolution diffusion imaging without compromising the SNR, a *patch-based super-resolution* retrospective method was used to increase the spatial resolution of the acquired diffusion-weighted images [20]. In addition to the super-resolution (sub-millimeter), we used the hybrid diffusion imaging (HYDI), which allows for fiber crossing delineation, to study the effects of aging on diffusion metrics in the hippocampal subfields and on structural connectivity between the subfields as well as between the hippocampus and the cortical brain regions.

Materials and Methods

Participants

In this feasibility study, five older healthy participants were recruited from the Indiana Alzheimer Disease Research Center (IADRC), and seven younger healthy participants were recruited from the community. The five older participants had an age greater than 65 years old (73 +/- 9.9 years), and the remaining seven participants had an age less than 35 years old (28.6 +/- 4.2 years). Each group had two male participants. Exclusion criteria for neuroimaging were significant cerebrovascular disease or malformations; a history of chemotherapy or radiation therapy; current major depression; a history of schizophrenia, bipolar disorder, developmental disability, Parkinson's disease, brain surgery, brain infection, or significant head injury (loss of consciousness > 30 min); and/or excessive alcohol consumption.

Older participants are a part of the Indiana Alzheimer's Disease Research Center (IADRC) cohort. They were cognitively normal (MMSE ≥18) at scan time. In addition, they underwent a comprehensive clinical assessment and neuropsychological battery, the complete details of which are listed in [21,22].

All procedures performed in studies involving human participants were in accordance with the ethical standards of the institutional Committee for the Protection of Human Subjects at Indiana University School of Medicine. In addition, all participants provided written informed consent according to procedures approved by the Institutional Committee for the Protection of Human Subjects at Indiana University School of Medicine (IRB no.: 1105005608 for older adults and 1407579759 for younger adults).

Imaging

MRI scans were performed on the participants in a Siemens MAGNETOM Prisma 3.0 T scanner and a 64-channel RF receiver head coil. High-resolution T1W images were acquired with an MPRAGE sequence at 0.8 x 0.8 x 0.8 mm^3 resolution, TR=2400 ms, TE=2.22 ms, TI=1000 ms, flip-angle=8°, 256 mm field-of-view, 208 slices, and GeneRalized Autocalibrating Partial Parallel Acquisition (GRAPPA) acceleration iPAT= 2.

A high-resolution Turbo-Spin-Echo T2W images were acquired with a high in-plane resolution of 0.4 x 0.4 mm in an oblique plane perpendicular to the main axis of the hippocampus, a slice thickness of 2 mm, TR=8310 ms, TE=50 ms, flip-angle=122°, 175 mm field-of-view, 32 slices, and GRAPPA acceleration iPAT=2.

HYDI [23,24] was performed with a single-shot spin-echo EPI sequence, a multiband factor of 3, TE=74.2 ms, and TR=4164 ms, 220 mm field of view, 114 slices, isotropic resolution of 1.25mm, and 10:51 (min: sec) acquisition time. The diffusion scheme included four shells of b-values 500, 800, 1600, 2600 s/mm^2, a total of 134 diffusion-directions, and 8 non-diffusion weighted volumes. Two sets of HYDI data were acquired with reversed phase-encoding blips for subsequent geometric distortion correction.

Preprocessing

All the diffusion-weighted images were denoised using overcomplete local-Principal-Component-Analysis as proposed in[25]. (FMRIB, Oxford, UK) Software Library v6.0 (FSL) tools, FSL-topup, and FSL-*eddy* [26] were used to correct motion, susceptibility, and eddy current distortions. Depending on when the motion happens in the HYDI scans, the motion artifacts may manifest in two different ways. When the head movement happens outside of the k-space reading, the motion artifacts present as rigid body displacements and can be retrospectively

corrected by image registration provided by the FSL *eddy* command. When the head movement happens during the k-space reading, the motion artifacts cause signal dropouts.

Because the diffusion MRI is a 2-dimensional (2D) imaging technique (i.e., individual 2D images/slices are acquired independently with one excitation pulse and one k-space reading for each image/slice). The signal dropouts could happen randomly to any slice in whole-brain image volumes. Slice-by-slice outlier detection functionality in FSL *eddy* could detect these dropout-slices and replace them with Gaussian Process predictions.

To achieve super-resolution, a collaborative-patch-based method dubbed as Collaborative and Locally Adaptive Super-Resolution (CLASR) [20] was used to bring the 1.25 mm^3 resolution HYDI data to a submillimeter resolution of 0.625 mm^3. This upsampling approach unveils fine structures by denoising the data with a Rician distribution in q-space (i.e., diffusion space). Therefore, unlike conventional upsampling approaches (e.g., zero filling), which do not add new information [27], this approach recovers underlying signals for subtle structures to achieve high resolution. The first two shells of the submillimeter HYDI data were used along with the FSL-DTIFIT command to compute DTI metrics. Then, all four HYDI shells were used to calculate the neurite orientation dispersion and density imaging (NODDI) [28] metrics using AMICO (https://github.com/daducci/AMICO_matlab) [29].

Postprocessing

Figure 1 shows the workflow of the algorithm pipeline of, which includes three main postprocessing steps: (1) segmentation of the hippocampal subfields; (2) FA-based registration of FSL-Harvard-Oxford cortical atlas to each subject and the parcellation of the cortical structural areas in the subject space (3) tractography using the super-resolution diffusion MRI; (4) Calculations of diffusion metrics and connectivity matrices of the hippocampal subfields.

The high-resolution T1W and T2W images were used for segmenting the hippocampal subfields with the Automatic Segmentation of Hippocampal Subfields (ASHS) method [30] version 1.0 [16] and the associated atlas: "ashs_atlas_upennpmc_20170810". The segmented hippocampal subfields were then transformed from the T2W image space to the super-resolution diffusion space using ANTs [31] which starts with affine registration using a 12-parameter linear registration (3 translations, 3 rotations, 3 scales, and 3 shears), followed by diffeomorphic or nonlinear registration.

Figure 2 illustrates an example of using the ASHS method along with the high-resolution T1W and T2W images of one young participant to segment the hippocampal subfields. The hippocampal subfields on the T2W image were then transformed to the b-value = 0 s/mm2 image in the super-resolution diffusion space using ANTs (34), as depicted in Figure 3a.

Tractography of the HYDI multi-shell data was reconstructed using the generalized q-sampling imaging (GQI) method [32]. This reconstruction used a deterministic fiber-tracking algorithm [33]. The parameters used in the reconstruction are the angular threshold of 35 degrees and the step size set to 0.1 mm. The fiber trajectories were smoothed by averaging the propagation direction with 10% of the previous direction. Tracks shorter than 3 mm or longer than 300 mm were discarded. A total of 800,000 tracts were calculated for each subject. For tractography within the hippocampus, the hippocampal subfields were used as seed and destination ROIs to filter the number of streamlines between each of the subfields. And for tractography from the hippocampus to the cortex, the whole hippocampus was used as the seed ROI and the parcellated cortical areas as designation ROIs.

Statistical analyses

This feasibility study assesses the method's ability to detect the correlation between age and the connectivity within the hippocampus, the connectivity from the hippocampus to the cortex. Thus, two types of analyses were performed: The first analysis was conducted using R-3.5 [34], where group comparisons were performed using unpaired two-samples Wilcoxon test with an FDR multiple-comparison correction of each diffusion metric; i.e., DTI maps: Fractional Anisotropy (FA), mean diffusivity (MD), axial diffusivity (Da), radial diffusivity (Dr) and NODDI maps: orientation dispersion (OD) and intracellular volume fraction (ICVF), comparing the younger group versus the older group. We performed regression analysis to test if the model accounting for gender and age explains the data significantly better than the model with age alone. Adding the gender did not have a significant effect, with a p-value exceeding 0.2 in all cases. We also tested the interaction between age and gender to see if the change in each group depends on gender. Again, there was no interaction between age and gender in each diffusion metric. A p-value < 0.05 was deemed significant in this analysis, after an FDR multiple comparisons.

The connectivity matrices were computed in the left and right hippocampal subfields and between the hippocampus and the cortex, using the mean of the number of streamlines between the subfields normalized by the volumes of the subfields involved in each connection. Second, a correlation analysis based on the number of streamlines connecting one subfield to another correlates with age among the twelve subjects. This analysis used the number of tractography streamlines normalized by the volume of the subfields involved in each connection as the dependent variable. We used the age of each participant as an independent variable in the same analysis.

Connectometry statistical analysis

To study the effect of aging on the hippocampus-cortex streamline connections, a group-wise connectometry analysis was used[35]. In this analysis, the diffusion data were reconstructed in the MNI space using q-space diffeomorphic reconstruction[36] to obtain the spin distribution function [32]. The output resolution of the resampling to the MNI space is 1 mm isotropic. The quantitative anisotropy (QA) was extracted as the local connectome fingerprint and used in the connectometry analysis. The analysis used the MNI-space hippocampal regions as ROIs [37].

Results

The results of the means and standard deviations of FA and MD in the left hippocampal subfields of one of the young participants are illustrated by Figure 3b. Figure 4 shows the group analysis of the diffusion metrics highlighting differences between the young and the older participants. Violin plots were used to visualize the diffusion metrics of each of the hippocampal subfields, including the cornu-ammonis subfields (CA1-3), dentate gyrus (DG), entorhinal cortex (ERC), and subiculum (SUB). The older participants had significantly lower DTI fractional anisotropy in the CA1 (p-value= 0.04197), CA2 (p-value= 0.03536), DG (p-value = 0.03536), and CA3 (p-value= 0.03536) (i.e., unpaired two-samples Wilcoxon test p-value < 0.05, after FDR multiple-comparison correction). While predominantly not significant, a trend of lower NODDI intracellular volume fraction (ICVF) was observed in older participants.

We were able to delineate the streamlines in the perforant pathway, which comprises fiber pathways connecting the entorhinal cortex and the hippocampal subfields, using the super-resolution submillimeter HYDI method. Figure 5 shows an approximation of the perforant pathway circuitry via tractography streamlines, representing the strength of the connection between the subfields in one of the younger subjects. This demonstrates the ability of the method to capture the connections among the hippocampal subfields, which was not possible with the original 1.25 mm data (Figure 6). However, in the case of the 1.25 mm^3 isotropic voxel

resolution, the connections between the subfields were extremely weak (as evident by the number of streamlines) due to the partial volume effects. Accordingly, no further analyses would deem useful in this resolution.

Connectivity matrices (i.e., connectomes) were computed between the subfields and between the hippocampus and the cerebral cortices in the form of normalized streamline counts. We compared the connectivity matrices in the left hippocampus using the isotropic resolution of 1.25 mm in the older and younger subjects versus their counterparts using the isotropic resolution of 0.0625 mm. Some of the connections are lost in the lower resolution matrices, which could be due to PVE in the lower resolution diffusion data.

To compare the connectivity in the hippocampus between the younger and older subjects, we used the number of streamlines between the subfields normalized by the volumes of the subfields involved in each connection. Figure 7 shows the mean connectivity matrices computed using this approach. These mean connectivity matrices were computed in the left and right hippocampal subfields in the older and younger groups. Similarly, Figure 8 shows the non-zero mean connectivity vectors from the left and right hippocampi to cortical regions for both age groups.

Pearson's correlation analysis between age and the number of streamlines connecting the hippocampal subfields is shown in Figure 9. To demonstrate the effect of sizes that are independent of the sample size, the strengths of correlations (either positive or negative) are also listed in the Figure. The results suggest that the number of streamlines was negatively correlated with the subjects' age in almost all the connections, especially in the left hippocampus.

And finally, the connectometry analysis depicted in Figure 10 shows that QA was negatively correlated with the subjects' age in each of the MNI-hippocampal ROIs with a false

discovery rate (FDR) that ranged between 0.0075 and 0.01. The negatively correlated tracks included: corpus callosum, left and right corticospinal tracts, left and right corticothalamic pathways, left and right cingulum, left and right fornix, left and right optic nerves, left and right inferior longitudinal fasciculus, left and right trochlear.

Discussion and Conclusion

This study achieved isotropic 0.625 mm resolution DWIs by applying the CLASR method to acquire 1.25 mm resolution DWIs without compromising the SNR. Furthermore, we could attain spatial super-resolution, which is essential to reduce the partial volume effects, and high angular resolution. This high angular resolution can delineate fiber crossings within the same voxel, providing more accurate tractography.

A possible extension of this work is to examine the difference of using GQI tracking scheme versus alternative tracking approaches such as Constrained spherical deconvolution (CSD) [38] to assess how that would affect the final results.

Most of the previous studies focused on using DTI to characterize the microstructural changes in the hippocampus[39-41]. However, it is known that DTI suffers severe limitations in regions of crossing fibers as the conventional tensor techniques cannot correspond to multiple, independent intra-voxel orientations.

In this study, we leveraged a super-resolution HYDI method with an analytical pipeline that can detect the strength of the connectivity in the form of streamlines count normalized by the volumes of the ROIs involved in the connection. Our results are supported by quantitative analysis using the correlation between the number of streamlines in the left and right hippocampal subfields versus age across all subjects (Figure 9). These results suggest that normal aging triggers differential effects in the connectivity in the hippocampal subfields. We

hypothesize that these differential effects might be more pronounced throughout different stages of AD. It has been recently demonstrated that using a multimodal approach that includes a super-resolution DTI could be used as a hippocampal subfield biomarker for AD detection [42].

This feasibility study indicates that the proposed pipeline can produce a new biomarker of aging. In this pipeline, the strengths of the connections characterized by the number of streamlines between the hippocampal subfields were reduced with age, especially in the left hippocampus. Although we focused on the hippocampus connections here, another extension of the method is to measure the connections between the cortical regions without involving the hippocampi.

As a feasibility study, the sample size of this study was modest. Thus, multiple comparison adjustments were not used, which might bias the results. Further work will focus on applying this method to a large cohort to study the relationship between structural connectivity and functional MRI activity in the entailed regions. This framework could help to discover new biomarkers that could be added to the comprehensive set of biomarkers of aging. This method holds promise for providing information regarding hippocampal integrity in the early stages of AD.

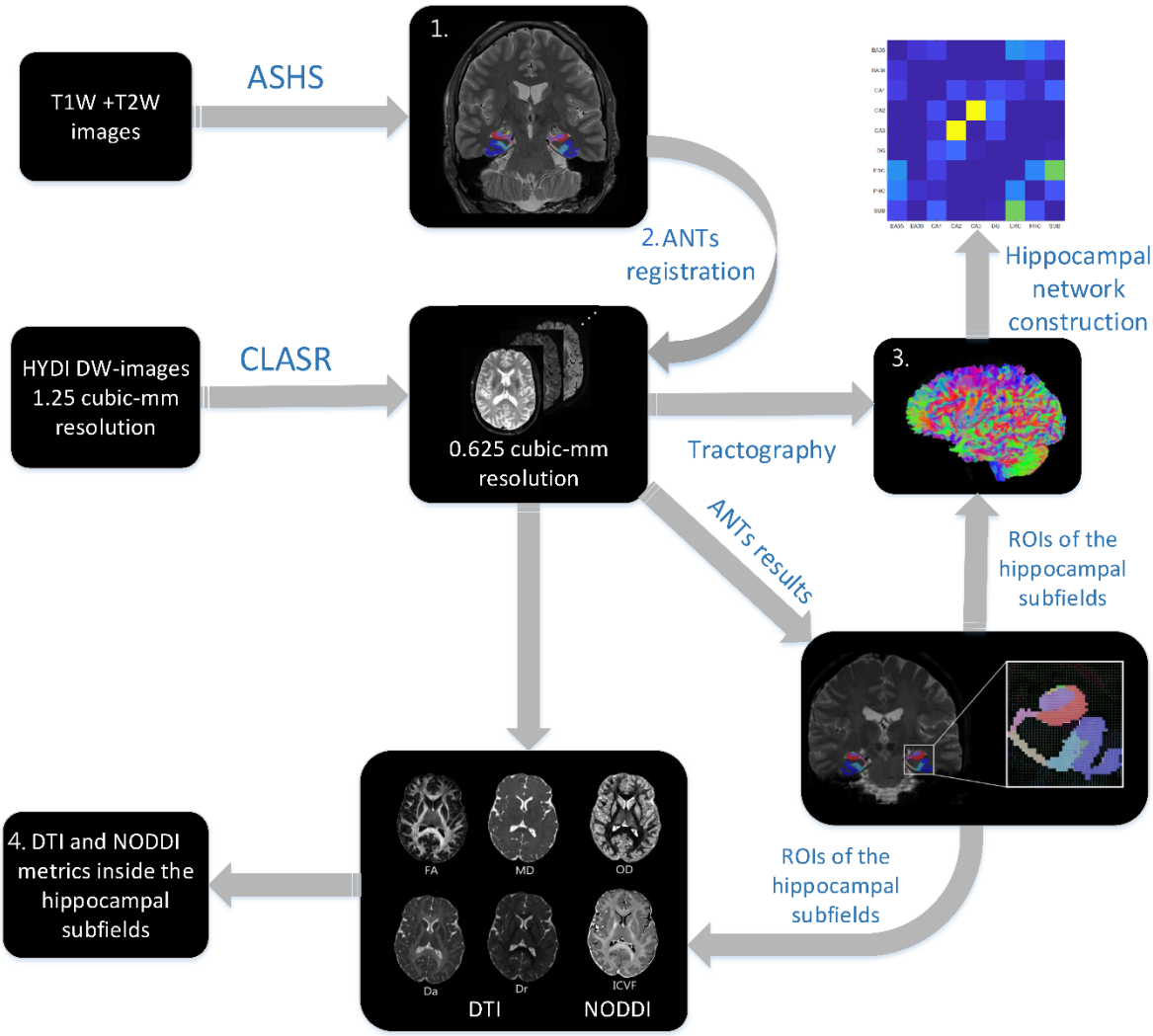

Figure 1. A framework of the analysis used in the hippocampal subfield network construction as well as computing the DTI and NODDI metrics inside the hippocampal subfields. The Automatic Segmentation of Hippocampal Subfields (ASHS) method (16) is used to segment the hippocampal subfields using the T1W and T2W images. Collaborative and locally adaptive super-resolution (CLASR) method was used to bring the 1.25 mm3 resolution HYDI data to a submillimeter resolution of 0.625 mm3. Masks of the regions of interests (ROIs) representing the hippocampal subfields were used to calculate the means and standard deviations inside the DTI and NODDI metrics. The same ROIs were used as seeds to produce the connectivity matrices that were calculated using the number of streamlines between those ROIs.

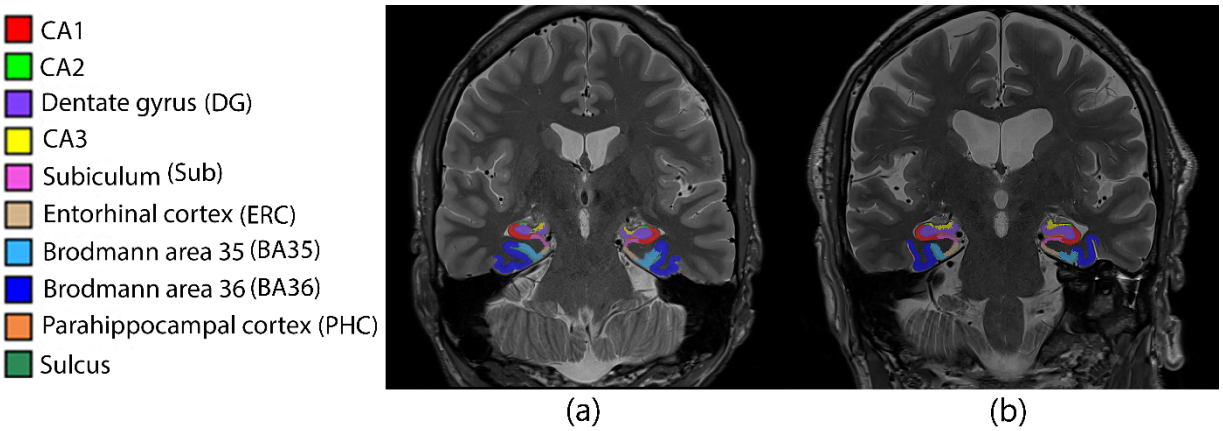

Figure 2. Two examples subjects with the hippocampal subfields segmented using the ASHS software overlaid on a T2-weighted image (T2W) of one younger subject (a) and one older

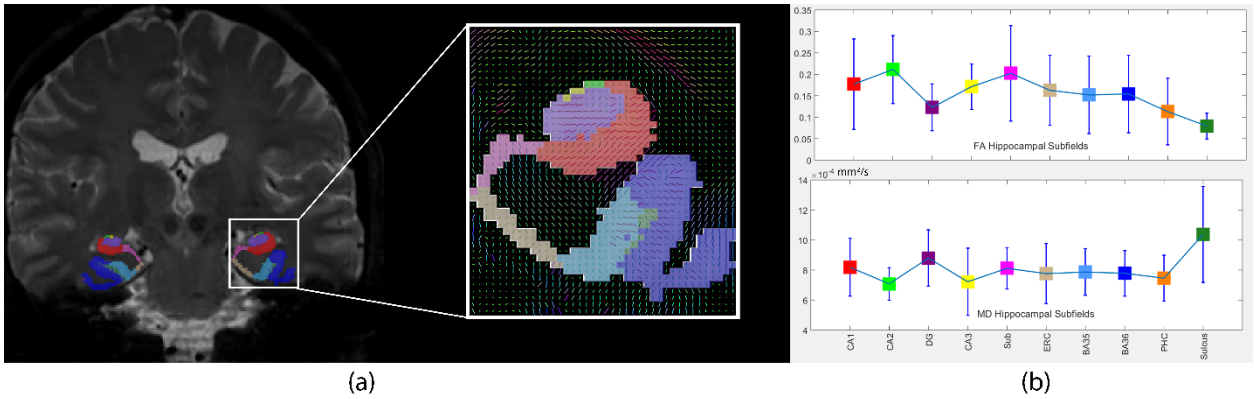

Figure 3. (a) Hippocampal subfields using the ASHS method then transformed to the diffusion-weighted image with a zoomed-in copy overlaid on an image of the major eigenvectors of the diffusion data. (b) Means and standard deviations of each of the FA and MD in the left hippocampal subfields shown in (a) in one young subject.

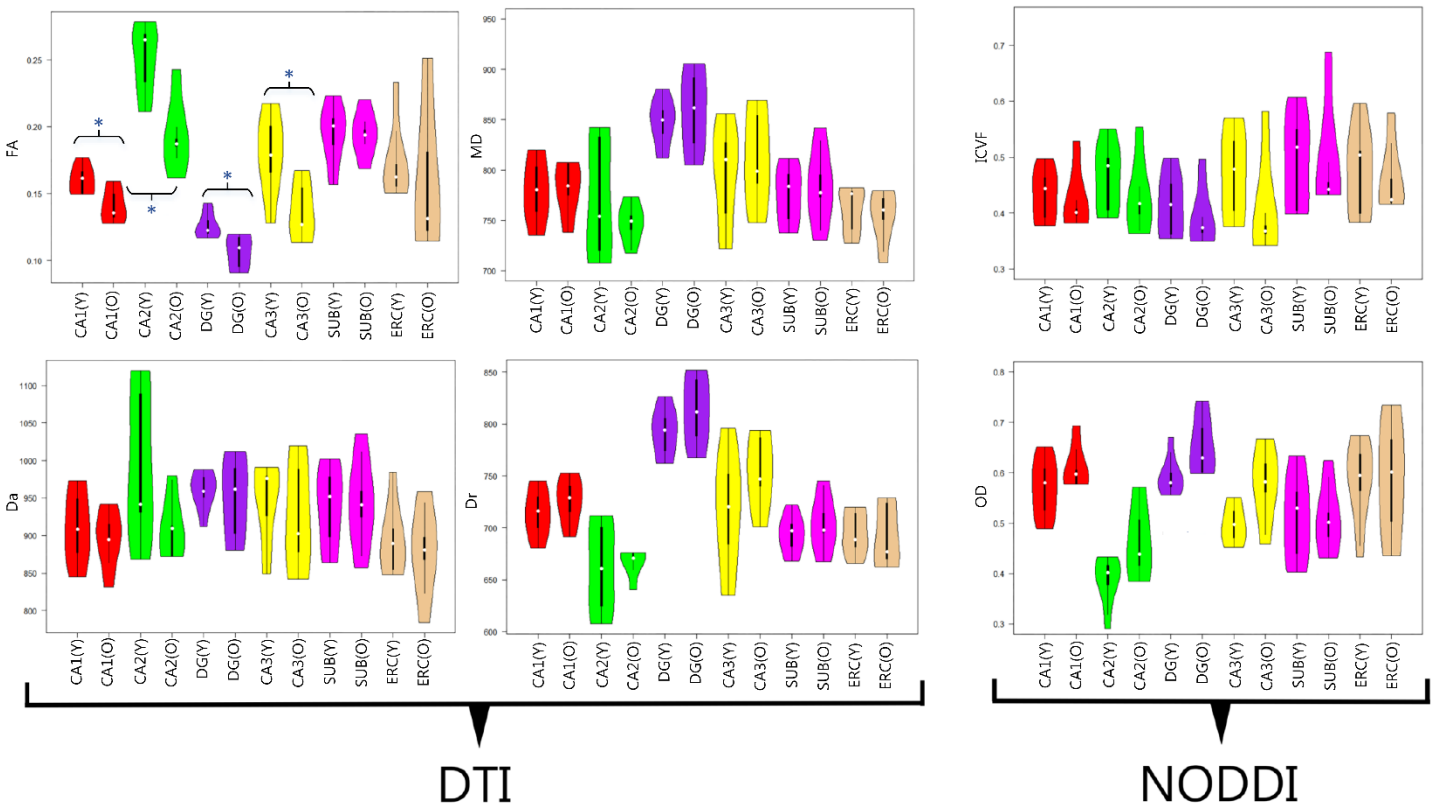

Figure 4. Violin plots showing diffusion metrics in both groups, the older group denoted by (O) and the younger group denoted by (Y) (i.e. DTI: FA, mean diffusivity (MD), axial diffusivity (Da), and radial diffusivity (Dr); and NODDI: orientation dispersion (OD) and intra-cellular volume fraction (ICVF)) between the older and younger groups inside the left hippocampal subfields. Unpaired two-samples Wilcoxon test was applied to compare the groups, significant differences (p-value <0.05) between the older and younger groups were found in the FA values of CA1, CA2, DG and CA3. There were no significant differences between the two groups in other diffusion metrics.

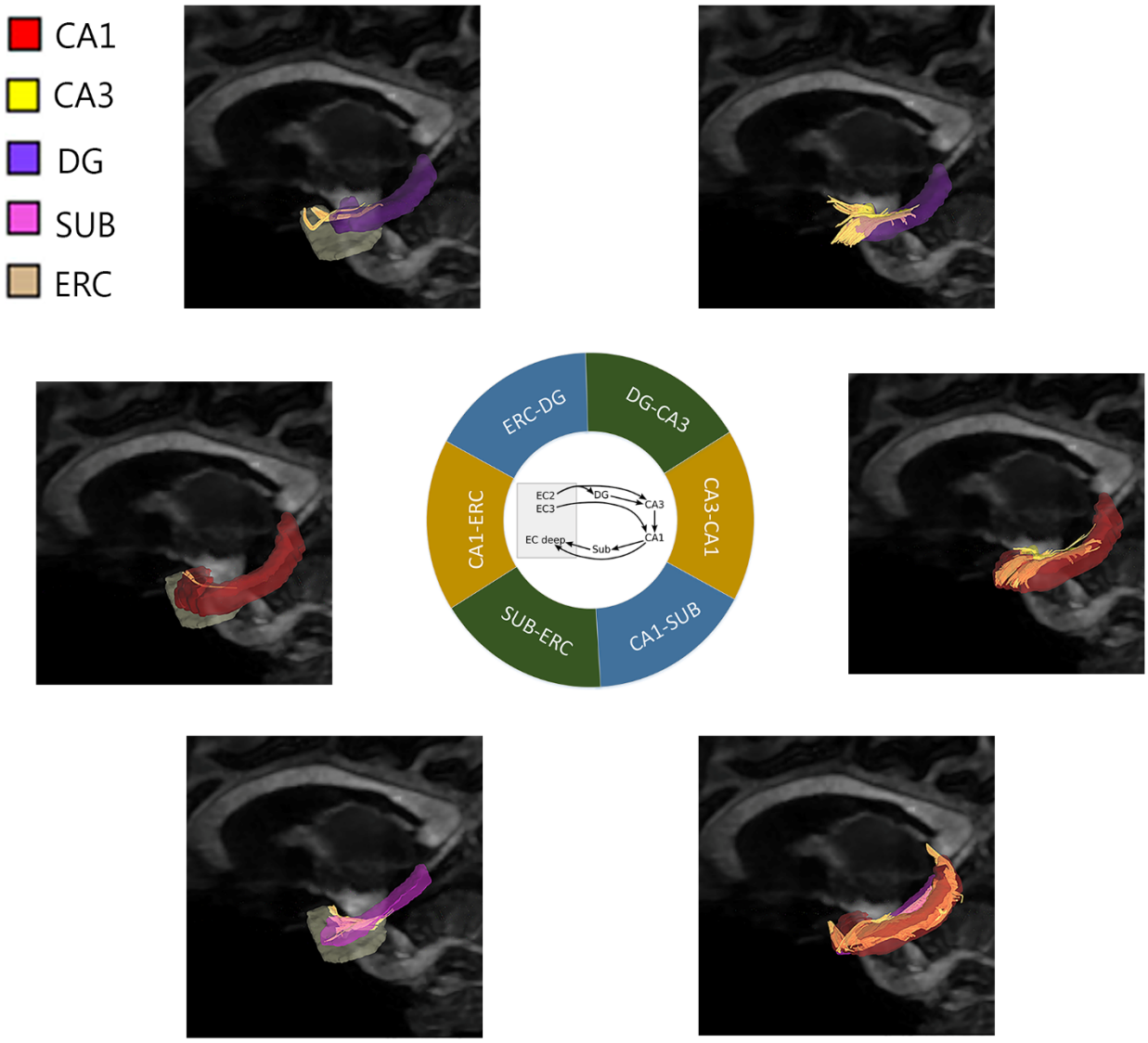

Figure 5. An approximation of the hippocampal connectivity circuit showing the perforant pathway connectivity in the form of streamlines in one of the younger subjects.

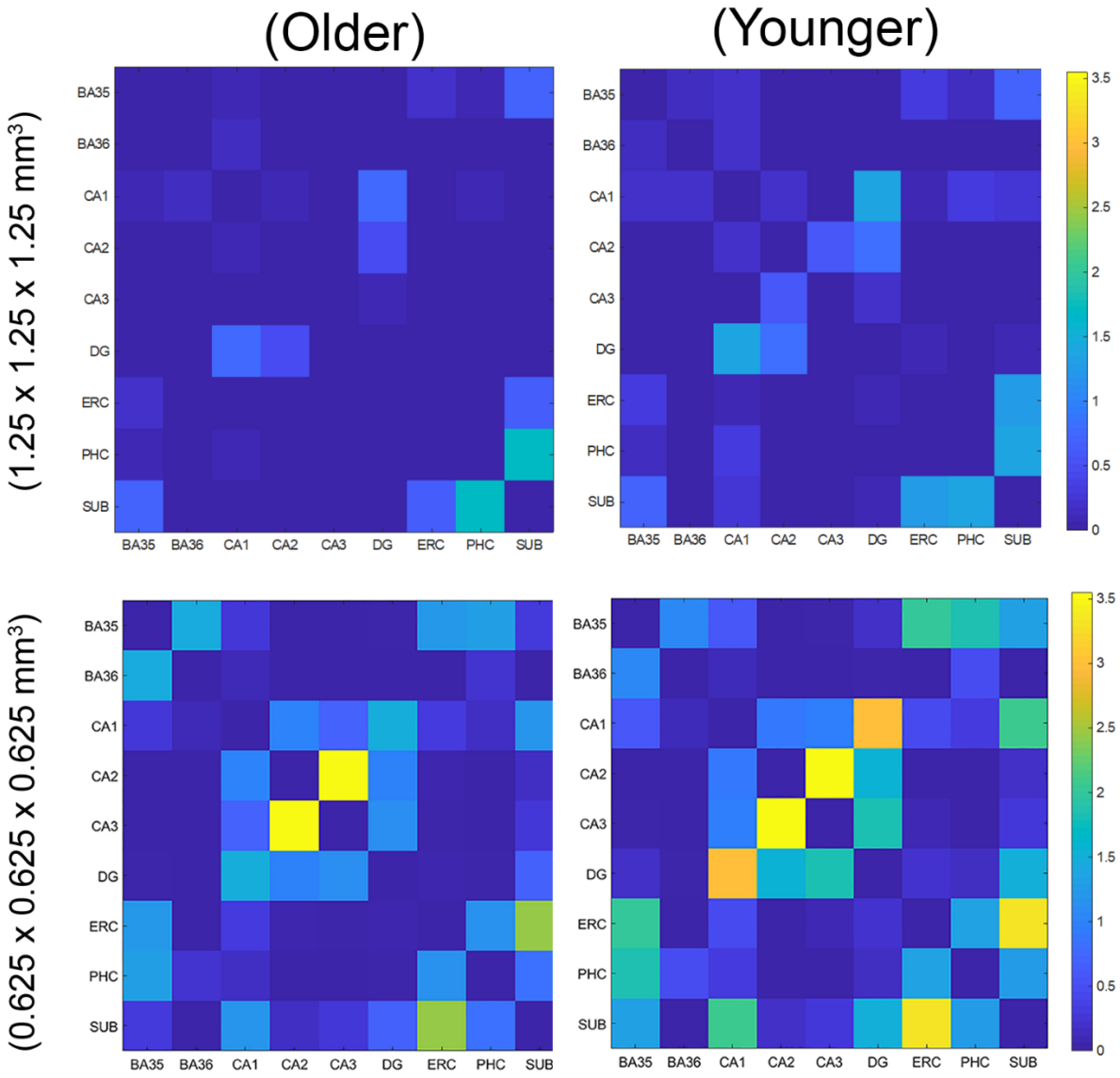

Figure 6. A comparison between the connectivity matrices of the left hippocampus produced by the isotropic resolution of 1.25 mm versus their counterparts produced by the isotropic resolution of 0.625 mm. In both cases the number of streamlines between the subfields normalized by the volumes of the subfields involved in each connection.

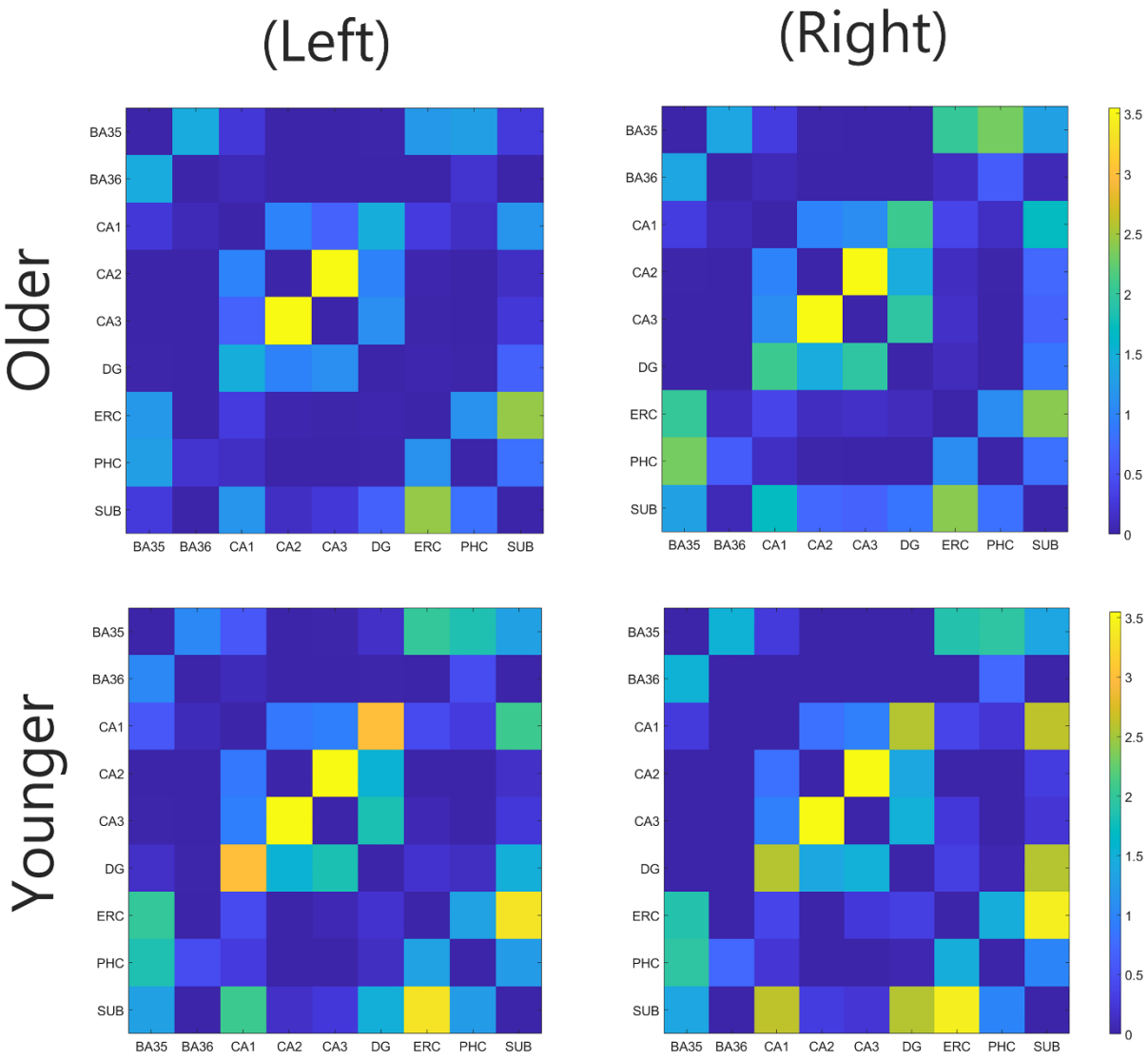

Figure 7. Connectivity matrices produced by the isotropic resolution of 0.625 mm of the left and right hippocampus using the mean of the number of streamlines between the subfields normalized by the volumes of the subfields involved in each connection.

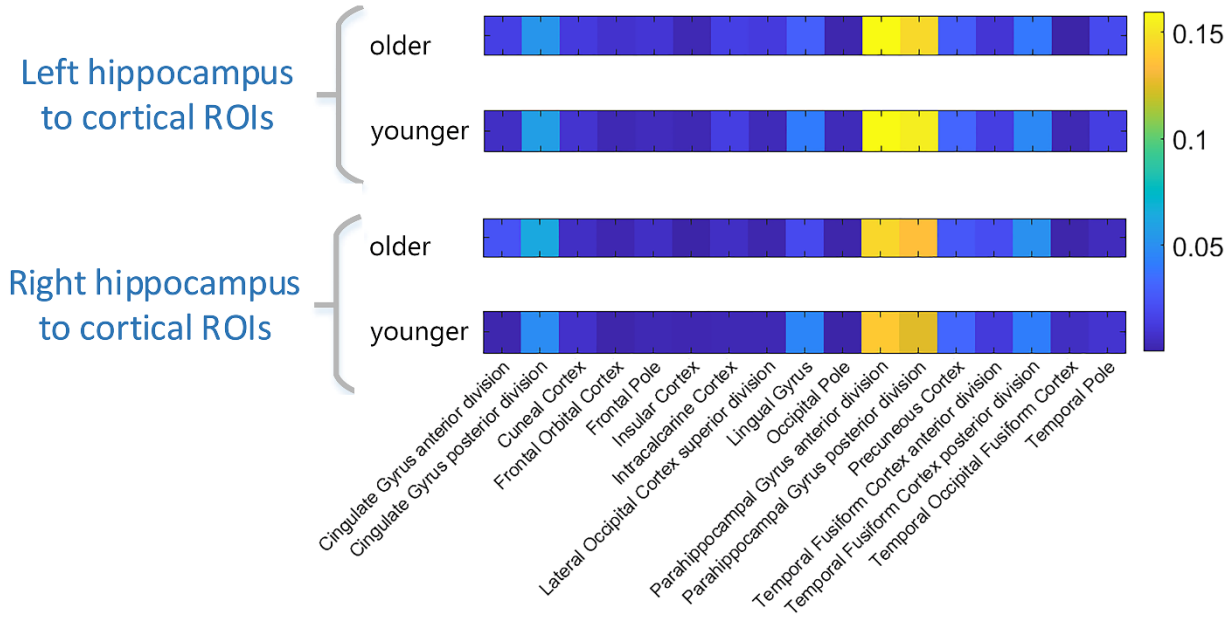

Figure 8. Number of streamlines from the left and right hippocampus to cortical ROIs normalized by the volumes of the ROIs involved in each connection.

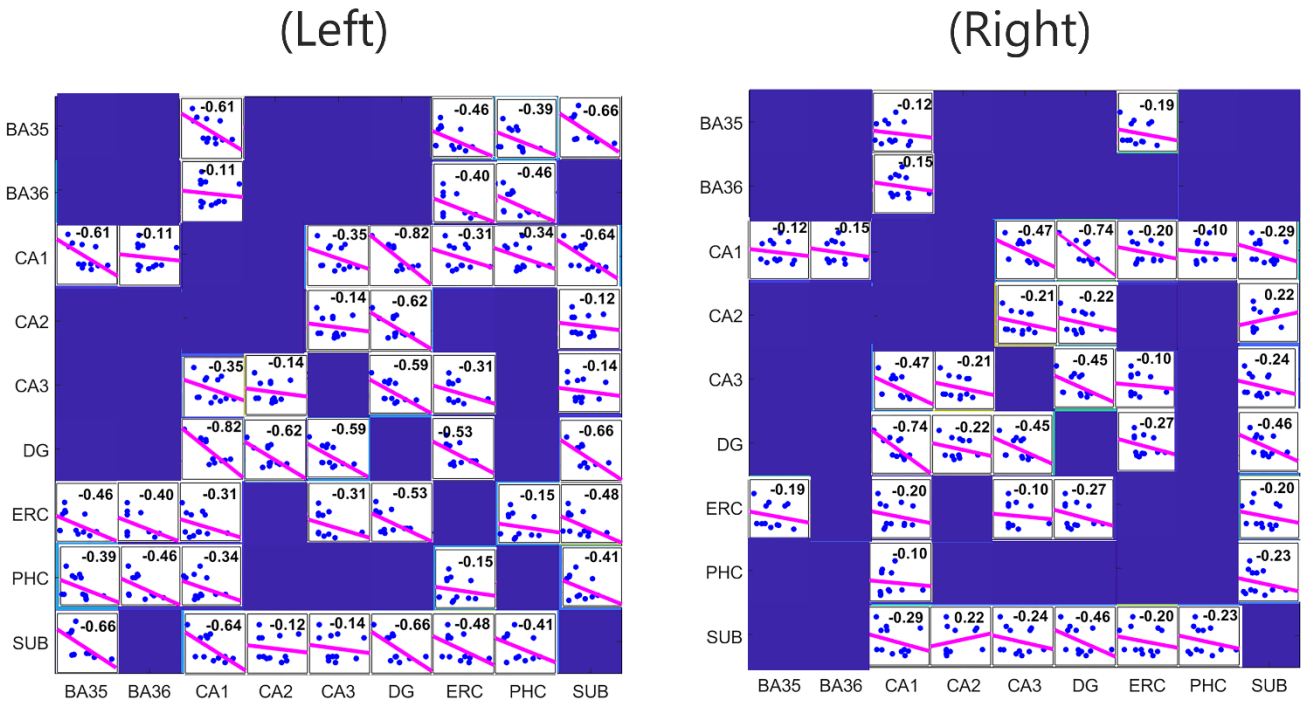

Figure 9. Correlation between the number of streamlines in the left and right hippocampal subfields versus age across the twelve subjects.

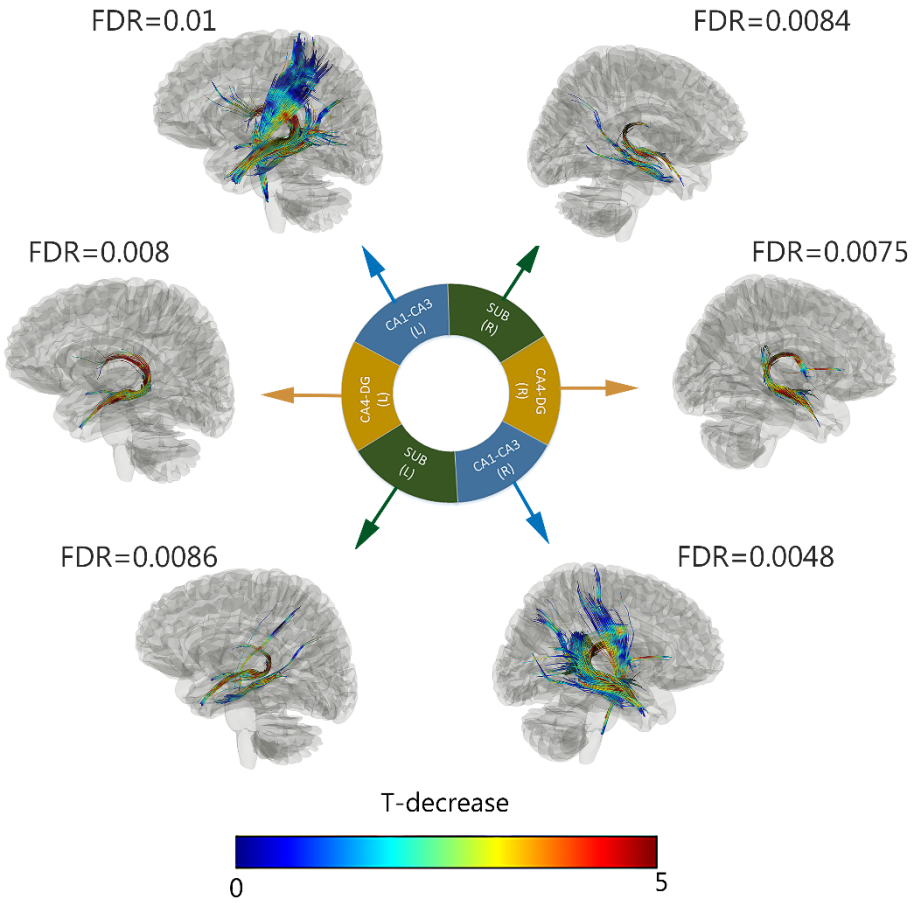

Figure 10.

Connectometry analysis showing that the quantitative anisotropy (QA) was negatively correlated with the subjects' age in each of the MNI hippocampalOIs with an FDR that ranges between (0.0075 and 0.01). The tracks are color-coded with T statistics related to a negative correlation.

References

1. Lupien S, Evans A, Lord C, et al. Hippocampal volume is as variable in young as in older adults: Implications for the notion of hippocampal atrophy in humans. *NeuroImage.* 2007;34(2):479-485.
2. Shing YL, Rodrigue K, Kennedy K, et al. Hippocampal Subfield Volumes: Age, Vascular Risk, and Correlation with Associative Memory. *Frontiers in Aging Neuroscience.* 2011;3(2).
3. Coupé P, Catheline G, Lanuza E, Manjón JV. Towards a unified analysis of brain maturation and aging across the entire lifespan: A MRI analysis. *Hum Brain Mapp.* 2017;38(11):5501-5518.
4. Flores RD, Joie RL, Chételat G. Structural imaging of hippocampal subfields in healthy aging and Alzheimer's disease. *Neuroscience.* 2015;309:29-50.
5. Mueller SG, Stables L, Du AT, et al. Measurement of hippocampal subfields and age-related changes with high resolution MRI at 4T. *Neurobiol Aging.* 2007;28(5):719-726.
6. Raz N, Gunning-Dixon F, Head D, Rodrigue KM, Williamson A, Acker JD. Aging, sexual dimorphism, and hemispheric asymmetry of the cerebral cortex: replicability of regional differences in volume. *Neurobiol Aging.* 2004;25(3):377-396.
7. Scahill RI, Frost C, Jenkins R, Whitwell JL, Rossor MN, Fox NC. A Longitudinal Study of Brain Volume Changes in Normal Aging Using Serial Registered Magnetic Resonance Imaging. *Archives of Neurology.* 2003;60(7):989-994.
8. Raz N, Ghisletta P, Rodrigue KM, Kennedy KM, Lindenberger U. Trajectories of brain aging in middle-aged and older adults: regional and individual differences. *Neuroimage.* 2010;51(2):501-511.

9. Pereira JB, Valls-Pedret C, Ros E, et al. Regional vulnerability of hippocampal subfields to aging measured by structural and diffusion MRI. *Hippocampus.* 2014;24(4):403-414.

10. Duvernoy HM. *The Human Hippocampus, Functional Anatomy, Vascularization, and Serial Sections with MRI.* Berlin, Germany: Springer; 1998.

11. Burggren AC, Zeineh MM, Ekstrom AD, et al. Reduced cortical thickness in hippocampal subregions among cognitively normal apolipoprotein E e4 carriers. *Neuroimage.* 2008;41(4):1177-1183.

12. Cong S, Risacher SL, West JD, et al. Volumetric comparison of hippocampal subfields extracted from 4-minute accelerated vs. 8-minute high-resolution T2-weighted 3T MRI scans. *Brain Imaging and Behavior.* 2018:1583-1595.

13. Iglesias JE, Augustinack JC, Nguyen K, et al. A computational atlas of the hippocampal formation using ex vivo, ultra-high resolution MRI: Application to adaptive segmentation of in vivo MRI. *NeuroImage.* 2015;115:117-137.

14. Van Leemput K, Bakkour A, Benner T, et al. Automated segmentation of hippocampal subfields from ultra-high resolution in vivo MRI. *Hippocampus.* 2009;19:549-557.

15. Yassa MA, Muftuler LT, Stark CE. Ultrahigh-resolution microstructural diffusion tensor imaging reveals perforant path degradation in aged humans in vivo. *Proc Natl Acad Sci U S A.* 2010;107(28):12687-12691.

16. Yushkevich PA, Pluta JB, Wang H, et al. Automated volumetry and regional thickness analysis of hippocampal subfields and medial temporal cortical structures in mild cognitive impairment. *Hum Brain Mapp.* 2015;36(1):258-287.

17. Zeineh MM, Holdsworth S, Skare S, Atlas SW, Bammer R. Ultra-high resolution diffusion tensor imaging of the microscopic pathways of the medial temporal lobe. *Neuroimage.* 2012;62(3):2065-2082.

18. Jones DK, Leemans A. Diffusion tensor imaging. *Methods Mol Biol.* 2011;711:127-144.

19. Mukherjee P, Chung SW, Berman JI, Hess CP, Henry RG. Diffusion Tensor MR Imaging and Fiber Tractography: Technical Considerations. *American Journal of Neuroradiology.* 2008;29(5):843-852.

20. Coupé P, Manjón J, Chamberland M, Descoteaux M, Hiba B. Collaborative patch-based super-resolution for diffusion-weighted images. *NeuroImage.* 2013;83:245-261.

21. Wen Q, Mustafi SM, Li J, et al. White matter alterations in early-stage Alzheimer's disease: A tract-specific study. *Alzheimers Dement (Amst).* 2019;11:576-587.

22. Contreras JA, Avena-Koenigsberger A, Risacher SL, et al. Resting state network modularity along the prodromal late onset Alzheimer's disease continuum. *NeuroImage: Clinical.* 2019;22:101687.

23. Wu Y-C, Alexander AL. Hybrid diffusion imaging. *NeuroImage.* 2007;36:617-629.

24. Wu Y-C, Field AS, Alexander AL. Computation of diffusion function measures in q-space using magnetic resonance hybrid diffusion imaging. *IEEE Trans Med Imaging.* 2008;27(6):858-865.

25. Manjón J, Coupé P, Concha L, Buades A, Collins D. Diffusion weighted image denoising using overcomplete local PCA. *PLoS ONE.* 2013;8(9).

26. Andersson J, Graham M, Zsoldos E, Sotiropoulos S. Incorporating outlier detection and replacement into a non-parametric framework for movement and distortion correction of diffusion MR images. *NeuroImage.* 2016;141:556-572.

27. Elsaid NMH, Wu Y. Super-Resolution Diffusion Tensor Imaging using SRCNN: A Feasibility Study*. Paper presented at: 2019 41st Annual International Conference of the IEEE Engineering in Medicine and Biology Society (EMBC); 23-27 July 2019, 2019.

28. Zhang H, Schneider T, Wheeler-Kingshott CA, Alexander DC. NODDI: practical in vivo neurite orientation dispersion and density imaging of the human brain. *Neuroimage.* 2012;61(4):1000-1016.

29. Daducci A, Canales-Rodriguez E, Zhang H, Dyrby T, Alexander D, Thiran J-P. Accelerated Microstructure Imaging via Convex Optimization (AMICO) from diffusion MRI data. *NeuroImage.* 2015:32-44.

30. Yushkevich PA, Wang H, Pluta J, et al. Nearly automatic segmentation of hippocampal subfields in in vivo focal T2-weighted MRI. *NeuroImage.* 2010;53(4):1208-1224.

31. Avants BB, Tustison N, Song G. Advanced normalization tools (ANTS). *Insight j.* 2009;2(365):1-35.

32. Yeh F, Wedeen V, Tseng W. Generalized q-sampling imaging. *IEEE Trans Med Imaging.* 2010;29:1626-1635.

33. Yeh F-C, Verstynen T, Wang Y, Fernández-Miranda J, Tseng W-YI. Deterministic diffusion fiber tracking improved by quantitative anisotropy. *PLOS ONE.* 2013;8(11):e80713.

34. A Language and Environment for Statistical Computing. *A Language and Environment for Statistical Computing.*2016.

35. Yeh FC, Vettel JM, Singh A, et al. Quantifying Differences and Similarities in Whole-Brain White Matter Architecture Using Local Connectome Fingerprints. *PLoS Comput Biol.* 2016;12(11):e1005203.

36. Yeh FC, Tseng WY. NTU-90: a high angular resolution brain atlas constructed by q-space diffeomorphic reconstruction. *NeuroImage.* 2011;58(1):91-99.

37. Kulaga-Yoskovitz J, Bernhardt BC, Hong SJ, et al. Multi-contrast submillimetric 3 Tesla hippocampal subfield segmentation protocol and dataset. *Sci Data.* 2015;2:150059.

38. Tournier JD, Calamante F, Gadian DG, Connelly A. Direct estimation of the fiber orientation density function from diffusion-weighted MRI data using spherical deconvolution. *NeuroImage.* 2004;23(3):1176-1185.

39. Rose S, Janke A, Chalk J. Gray and white matter changes in Alzheimer's disease: a diffusion tensor imaging study. *Journal of Magnetic Resonance Imaging.* 2008:20-26.

40. Yassa MA, Muftuler LT, Stark CEL. Ultrahigh-resolution microstructural diffusion tensor imaging reveals perforant path degradation in aged humans in vivo. *PNAS.* 2010;107(28):12687–12691.

41. Zeineh MM, Holdsworth S, Skare S, Atlas SW, Bammer R. Ultra-high resolution diffusion tensor imaging of the microscopic pathways of the medial temporal lobe. *NeuroImage.* 2012:2065-2082.

42. Hett K, Ta V, Catheline G, et al. Multimodal Hippocampal Subfield Grading For Alzheimer's Disease Classification. *Scientific Reports.* 2019:13845.